

# Polymer Braids and Iterated Moiré Maps

David R. Nelson

*Lyman Laboratory of Physics, Harvard University, Cambridge, MA 02138*

and

Randall D. Kamien

*School of Natural Sciences, Institute for Advanced Study, Princeton, NJ 08540*

Crystalline order in dense packings of long polymers with a definite handedness is difficult to reconcile with the tendency of these chiral objects to twist and braid about each other. If the chirality is weak, the state of lowest energy is a triangular lattice of rigid rods. When the chirality is strong, however, screw dislocations proliferate, leading to either a tilt grain boundary phase or a new “moiré state” with twisted bond order. In the latter case, polymer trajectories in the plane perpendicular to their average direction are described by iterated moiré maps of remarkable complexity, reminiscent of dynamical systems.

28 December 1994

---

To Appear in the *Proceedings of the Wiener 1994 Centennial Symposium* edited by D. Jerison, I.M. Singer and D.W. Strock

## 1. Introduction

A notable feature of biological materials is the profusion of long polymer molecules with a definite handedness. DNA, polypeptides (such as poly- $\gamma$ -benzyl-glutamate) and polysaccharides (such as xanthan) can all be synthesized with a preferred chirality. Long polymers in dense solution often crystallize into a hexagonal columnar phase, *i.e.*, a lattice of rod-like objects with the cross section a triangular lattice. When the polymers are chiral this close packing into a triangular lattice competes with the tendency for the polymers to twist macroscopically [1] as in cholesteric liquid crystals. Similar to the twist grain boundary phase of chiral smectics [2], macroscopic chirality can proliferate when screw dislocations enter the crystal. Though the screw dislocations cost a finite energy, when the energy increase is offset by the decrease in free energy from twisting, the screw dislocations will penetrate the sample. If the chirality is weak, a defect free hexagonal columnar phase persists.

In this note we discuss the effect of chirality on the hexagonal columnar phases [3] of long polymers [4]. We neglect for simplicity heterogeneity along the polymer backbones and work with a two component displacement field perpendicular to the local polymer direction. The usual chiral term relevant for cholesteric liquid crystals produces a polymer tilt grain boundary phase, similar to the smectic- $A^*$  phase [2]. We find, as well, an additional term in the free energy which favors the rotation of the bond order along the average polymer direction. This term leads to braided polymers with twisting describable by a sequence of moiré patterns. The polymer braids can be described by a map from one perfect crystalline lattice to another perfect lattice rotated by a relative angle  $\phi$  and separated by honeycomb network of defects. When  $\phi$  takes on certain lock-in angles, the free energy of the crystal distortion will go through a minimum. The resulting map creates moiré patterns when the monomer locations are projected down the polymer axes. Upon iteration, corresponding to many periodically spaced defect walls, these moiré maps exhibit complex, self-similar

behavior, reminiscent of chaotic dynamical systems. Little appears to be known about the properties of these iterated moiré maps.

In the next section we review the continuum elastic theory which applies to a polymer crystal. We show how the energy of dislocation defects in the crystal determines the critical values of the chiral coupling constants at which chirality first enters. We describe the smectic twist grain boundary state as well as its polymer analogue, the tilt grain boundary state. In the last section we describe a microscopic model of the moiré phases, and discuss the lock-in angles which will produce moiré maps and braided polymer crystals. Finally, in the appendix we prove that any rotation angle of a crystal which produces a non-trivial coincidence lattice (as do the special lock-in angles discussed above) is an irrational fraction of  $2\pi$ .

## 2. Statistical Mechanical Model and the Tilt Grain Boundary Phase

In order to calculate averages of physical quantities, we integrate over the ensemble of all states, with each state weighted by the Boltzmann weight

$$P[\vec{u}] = \mathcal{Z}^{-1} \exp\{-F[\vec{u}]/k_{\text{B}}T\} \quad (2.1)$$

where  $\vec{u}(x_1, x_2, x_3)$  is the two-dimensional displacement field of the polymers from a perfect triangular lattice of rods, and  $\mathcal{Z}$  is the partition function. The elastic free energy, appropriate for a crystalline state of polymers lying on average along the  $z$ -axis, is

$$F[\vec{u}] = \int d^3x \left\{ \mu u_{ij}^2 + \frac{\lambda}{2} u_{ii}^2 + K_3 (\partial_z^2 u_i)^2 - \gamma \nabla_{\perp} \times \delta \vec{n} - \gamma' \partial_z \theta_6 \right\} \quad (2.2)$$

where  $u_{ij} = \frac{1}{2}(\partial_i u_j + \partial_j u_i)$ ,  $\delta n_i = \partial_z u_i$ , and  $\theta_6 = \frac{1}{2} \epsilon_{\mu\nu\rho} n_{\mu} \partial_{\nu} u_{\rho} = \frac{1}{2} \epsilon_{ij} \partial_i u_j$  in the nematic ( $\vec{n}_0 = \hat{z}$ ) ground state. These fields measure respectively the local strain, tilt and bond order of the crystal. Here and throughout Roman indices run from 1 to 2 while Greek indices run from 1 to 3. Terms which are not invariant under spatial reflection are chiral and are not allowed in systems with mirror symmetry. The last two terms in (2.2) are the

only allowed couplings in a chiral polymer system to lowest order in the gradients of  $\vec{u}$ . The term proportional to  $\nabla_{\perp} \times \delta \vec{n}$  favors a cholesteric-like twisting [3] of the local polymer direction along a pitch axis, perpendicular to the planes in which the polymers, on average, lie. The term proportional to  $\partial_z \theta_6$  favors a twisting of the bond order along the polymer direction. This term, and its effect on the polymer trajectories, can be described by moiré maps. In the columnar crystal the two chiral terms are the same if  $\partial_z \partial_i = \partial_i \partial_z$ . However, in the presence of crystal dislocations derivatives do *not* commute,  $\nabla_{\perp} \times \delta \vec{n} = \epsilon_{ij} \partial_i \partial_z u_j \neq \partial_z \epsilon_{ij} \partial_i u_j = \partial_z \theta_6$ . A dislocation line is characterized by the value of the line integral around this defect [5]

$$\oint_{\Gamma} ds_{\mu} \partial_{\mu} u_i = -b_i \quad (2.3)$$

where  $\vec{b}$  is the Burgers vector. The Burgers vector must be an integer linear combination of lattice vectors. It points parallel to the defect axis for the screw dislocation shown in Figure 1.

Various arrangements of dislocations lead to the twisting and braiding of polymers favored by  $\gamma$  and  $\gamma'$ . Burgers vectors of dislocations in a hexagonal columnar phase lie in the  $xy$ -plane, and there are three generic types [3]: a screw dislocation, an edge dislocation with tangent along  $\hat{z}$ , and an edge dislocation lying in the  $xy$ -plane. The latter defect requires aligned polymer ends which we can neglect if the polymers are very long. The remaining dislocations must lie in a plane spanned by their Burgers vector  $\vec{b}$  and  $\hat{z}$ , which amounts to choosing dislocation complexions with  $\alpha_{xy} = \alpha_{yx}$ , where the dislocation density tensor  $\alpha_{\gamma i}$  is the density of dislocations with tangents along the  $\gamma$ -direction with Burgers vectors pointing in the  $i$  direction [6].

Proceeding as in [5,6] we introduce a new field  $w_{\gamma i} \equiv \partial_{\gamma} u_i$  away from any dislocations. The non-commutivity of the derivatives of  $\vec{u}$  is represented by the dislocation density,  $\epsilon_{\mu\nu\gamma} \partial_{\nu} w_{\gamma i} = -\alpha_{\mu i}$ . One can solve for  $w_{\gamma i}$  in terms of the dislocation density  $\alpha_{\gamma i}$  and find the equilibrium displacement field in the presence of crystal defects [4]. In terms of the nematic and bond order field non-commutivity of derivatives means  $2\partial_z \theta_6 - \nabla_{\perp} \times \delta \vec{n} =$

$-\text{Tr}[\alpha]$ . The energy per unit length  $f_s$  of a screw dislocation is finite, while that of an edge dislocation lying along the  $\hat{z}$  direction diverges logarithmically with system size [7]. A screw dislocation is illustrated in Figure 1. Depending on how the dislocations are combined together a screw dislocation array can either produce a non-vanishing  $\nabla_{\perp} \times \delta\vec{n}$  or  $\partial_z\theta_6$ . Our predictions for the phase diagram as a function of  $\gamma$  and  $\gamma'$  are summarized in Figure 6.

If the chirality is strong and  $\gamma \gg \gamma'$  we expect the polymer analogue of the Renn-Lubensky twist-grain-boundary state [2] of chiral smectic liquid crystals. Smectic liquid crystals are, in some sense, dual to the hexagonal columnar phases considered here [3]. Smectics are composed of sheets of rod-like molecules; they are crystalline in one direction (the direction perpendicular to the layers) instead of two. If the molecules are chiral these layers want to twist, thus disrupting the crystalline order. At low chiralities, macroscopic twist is suppressed. Above a certain threshold chirality, screw dislocations enter the sample, causing the smectic slabs to undergo, on average, a uniform rotation along a direction perpendicular to the layer normals. In Figure 2 we show the structure of this state. Polymer crystals, as well, can have a state characterized by a constant overall twist perpendicular to the polymer axes. The state consists of a parallel array of tilt grain boundaries, separated by  $d'$  along the rotation axis, bounding regions of perfect polymer crystals similar to the smectic planes in Figure 2. Each of these tilt grain boundaries (TGB) is composed of a parallel array of screw dislocations lying, say, in the  $xz$ -plane, pointing along the  $x$ -axis and uniformly spaced along  $\hat{z}$  with spacing  $d$ . As illustrated in the upper inset of Figure 6 this dislocation texture causes a discrete rotation  $\phi = \tan^{-1}(b/d)$  (with  $b = a_0$ , corresponding to the shortest allowed Burgers vector) in the average polymer direction across the boundary. The spatial integral of  $\nabla_{\perp} \times \delta\vec{n}$  is non-zero, while the integral of  $\partial_z\theta_6$  vanishes. The TGB state appears when the chiral coupling  $\gamma$  exceeds the critical value  $\gamma_c = f_s/b$  [4].

### 3. The Moiré State

The second chiral coupling  $\gamma'$  has no analogue in chiral smectics. To find a configuration of screw dislocations which exploits this form of chirality we search for a dislocation texture which produces a displacement depending only on  $z$ . The only texture which does not produce divergent elastic energy is one in which the only non-zero components of  $\alpha_{\gamma i}$  are  $\alpha_{xx} = \alpha_{yy}$  [6,4]. A honeycomb array of screw dislocations, on average, produces this dislocation texture. We now find that for a single such grain boundary  $\nabla_{\perp} \times \delta \vec{n}$  vanishes far from the boundary while  $\partial_z \theta_6$  does not. This sort of grain boundary thus causes a net twist of the hexatic bond order parameter  $\theta_6$  while imposing no net  $\nabla_{\perp} \times \delta \vec{n}$ . When  $\gamma' \gg \gamma$  and the chirality is large, screw dislocations penetrate for  $\gamma' > \gamma'_c = 2f_s/b$ . By choosing the rotation angle across the honeycomb dislocation network to produce a high density of coincidence lattice sites [8] we produce especially low strain energies across the boundary. The superposition of triangular polymer lattices below and above the boundary forms a moiré pattern. The superposition of many such “moiré sheets” along the  $z$ -axis braids the polymers with deep minima in the energy at certain lock-in angles. Figure 3 illustrates the mapping of polymers across the moiré plane. Polymers in the lower half-space (circles) must be connected to the closest available polymer in the upper half-space (crosses) to minimize bending energy. Note that the map has a discrete translational symmetry, in the sense that any coincidence site could be a center of rotation. Especially simple moiré maps arise for the rotation angles

$$\phi_n = 2 \tan^{-1} \left[ \frac{\sqrt{3}}{3(2n+1)} \right] \quad (3.1)$$

$n = 1, 2, \dots$ . Figure 3 shows these maps for  $n = 1, \dots, 4$ . It is shown in Appendix A that all such angles are irrational fractions of  $2\pi$  [4] so that the structure never repeats upon iteration. Around each coincidence point there are  $n$  concentric rings of helical polymers. The lattice of coincidence points is also a triangular lattice, but with a spacing  $a_n = a_0 \sqrt{1 + 3(2n+1)^2}/2$ , where  $a_0$  is the original lattice constant. The geometrical

origin of such energetically preferred lock-in angles has no analogue in chiral smectics. The exact choice of lock-in angles and spacing between moiré planes must be settled by detailed energetic calculations.

Upon two iterations of the moiré map separating three regions of polymer crystal, the first coincidence lattice is rotated with respect to the second coincidence lattice by precisely the angle of rotation  $\phi_n$ . Thus the composite coincidence lattice is the “coincidence lattice of coincidence lattices”, with lattice constant  $a_n^2/a_0$ . Moiré maps iterated  $p$  times lead to triangular composite coincidence lattices with spacing  $a_n(a_n/a_0)^{p-1}$ , i.e. to ever sparser lattices of fixed points with intricate fractal structure in between them. Figure 4 shows the projected polymer paths for a lock-in angle of a square lattice (with  $\phi_1 = \tan^{-1}(3/4) \approx 36.9^\circ$ ) iterated  $p = 1, \dots, 4$  times. For a square lattice an especially simple sequence of lock-in angles is given by

$$\phi_n^{\text{square}} = \tan^{-1} \left[ \frac{2n+1}{2n(n+1)} \right], \quad (3.2)$$

leading to coincidence lattice spacings  $a_n^{\text{square}} = a_0 \sqrt{n^2 + (n+1)^2}$ .

In contrast to the TGB state polymers for  $p \gg 1$  are highly entangled and wander far from straight line trajectories. The polymer configurations and the dislocations leading to them are shown in Figure 5 for the  $n = 1$  moiré map of a triangular lattice iterated nine times. Near the moiré planes both  $\theta_6$  and  $\nabla_{\perp} \times \delta \vec{n}$  are nonzero. The center polymer is a fixed point of all the maps. Any such fixed polymer has a halo of others twisting around it. In this special tube, the nematic order parameter takes on the texture of a double twist cylinder as found in the low-chirality limit of blue phases of cholesteric liquid crystals [9]. The moiré state takes advantage of both double twist energies and the new chiral coupling  $\gamma'$ .

The phase diagram in Figure 6 summarizes our conclusions. As for chiral smectics [2], it is possible to cast the theory in a form similar to the Ginzburg-Landau theory of Type II superconductors in a magnetic field [4]. The couplings  $\gamma$  and  $\gamma'$  represent two distinct “magnetic fields” in this analogy. The hexagonal columnar phase expels all macroscopic

chirality. The two chiral couplings  $\gamma$  and  $\gamma'$  cause screw dislocations to penetrate the crystal above critical strengths  $\gamma_c$  and  $\gamma'_c$ , similar to the penetration of Abrikosov vortices above the lower critical field  $H_{c1}$ . The TGB phase predicted here for chiral polymers is similar to that already observed experimentally in chiral smectics [2]. The braided moiré state is qualitatively new, and its experimental observation would be of considerable interest. In Figure 7 we show 40 random polymers subject to 99 iterations of the  $n = 1$  map for the triangular lattice, all near a central, fixed coincidence lattice point. Surprising little is known about the intricate trajectories produced by such iterated moiré maps. These could be studied experimentally via neutron diffraction in hexagonal columnar crystals with a dilute concentration of deuterated polymer strands. Numerical studies of the local fractal dimension and Lyapunov exponent of these polymer trajectories are currently in progress.

#### 4. Acknowledgements

It is a pleasure to acknowledge stimulating conversations with T. Lubensky, R. Meyer, P. Taylor, E. Thomas, and J. Toner. DRN acknowledges the hospitality of Brandeis University, AT&T Bell Laboratories, and Exxon Research and Engineering, as well as support from the Guggenheim Foundation and the National Science Foundation Grant No. DMR-94-17047, and in part through the Harvard Materials Research Science and Engineering Center, under Grant No. DMR-94-17047. RDK was supported by National Science Foundation Grant No. PHY92-45317

#### Appendix A. Irrationality of the Lock-In Angles

The special lock in angles that we have found for the triangular lattice are all irrational fractions of  $2\pi$ . We will prove a more general theorem in this appendix that applies to any rotation which leads to a coincidence lattice with a finite lattice constant.

Let  $\mathbf{R}(\theta, \Lambda) = \Lambda'$  be the lattice generated by rotating a lattice of points  $\Lambda$  by  $\theta$  around a lattice site at the origin. Consider a regular lattice  $\Lambda_1$ , a set of ordered pairs



$\{(x_1, y_1), (x_2, y_2), \dots\}$ . Suppose there is an angle  $\theta^*$  for which the intersection of  $\Lambda_1$  and  $\mathbf{R}(\theta^*, \Lambda_1)$  is a lattice (not equal, as in the pathological case  $\Lambda_1 = \mathbf{R}(\theta^*, \Lambda_1)$ , to the original lattice) with a finite lattice constant. These angles are special lock-in angles which keep a finite fraction of polymers from stretching. Let  $\Lambda_1^n = \mathbf{R}(n\theta^*, \Lambda_1)$ . Let the intersection of  $\Lambda_1^0$  and  $\Lambda_1^1$  be the coincidence lattice  $\Lambda_2^0$ , and similarly  $\bigcap_{j=m}^{m+k} \Lambda_1^j = \Lambda_{k+1}^m$ . Note that  $\Lambda_k^m = \mathbf{R}(m\theta^*, \Lambda_k^0)$ . The intersection of  $\Lambda_1^1$  and  $\Lambda_1^2$  is also a coincidence lattice, but as  $\Lambda_1^1$  and  $\Lambda_1^2$  are rotated by  $\theta^*$  from  $\Lambda_1^0$  and  $\Lambda_1^1$ , respectively, their intersection,  $\Lambda_2^1$  will be rotated by  $\theta^*$  from  $\Lambda_2^0$ . Thus, since the intersection of  $\Lambda_1^0$ ,  $\Lambda_1^1$  and  $\Lambda_1^2$  is just the intersection of  $\Lambda_2^0$  and  $\Lambda_2^1$  the resulting coincidence lattice is the coincidence lattice of the coincidence lattices  $\Lambda_2$ .

In general, if we look at  $\Lambda_{n+1}^0$

$$\Lambda_{n+1}^0 \equiv \bigcap_{j=0}^n \Lambda_1^j = \left( \bigcap_{j=0}^{n-1} \Lambda_1^j \right) \cap \left( \bigcap_{j=1}^n \Lambda_1^j \right) \equiv \Lambda_n^0 \cap \mathbf{R}(\theta^*, \Lambda_n^0). \quad (\text{A.1})$$

Thus  $\Lambda_{n+1}^0$  is the coincidence lattice of two coincidence lattices  $\Lambda_n$ . Therefore as we add layer after layer, consecutively rotating by  $\theta^*$  we will produce ever sparser lattices with growing lattice constants.

Now assume that  $\theta^*$  is a rational fraction of  $2\pi$ , so  $\theta^* = 2\pi \frac{p}{q}$ . Then, after  $q$  iterations of the rotation the lattices would repeat, or, in other words,  $\Lambda_1^q = \Lambda_1^0$ . This would mean that  $\Lambda_{q+1}^0 \equiv \bigcap_{j=0}^q \Lambda_1^j = \bigcap_{j=0}^{q-1} \Lambda_1^j \equiv \Lambda_q^0$  since  $\Lambda_1^q$  has already been included in the intersection of the first  $q$  lattices. This contradicts the conclusion of the preceding paragraph. Therefore it is impossible to have a rotation angle  $\theta^*$  which is both a rational fraction of  $2\pi$  and produces a coincidence lattice with a non-trivial but finite lattice constant. Thus all lock-in angles must be irrational fractions of  $2\pi$ , which is what we were to prove.

## References

- [1] F. Livolant and Y. Bouligand, *J. Phys. (Paris)* **47** 1813 (1986); For tilt and moiré boundaries in the non-biological polymer PBZO (poly-paraphenylene benzobisoxazole) see D.C. Martin and E.L. Thomas, *Phil. Mag. A* **64**, 903 (1991).
- [2] S.R. Renn and T.C. Lubensky, *Phys. Rev. A* **38**, 2132 (1988); For experiments, see G. Srajer, R. Pindak, M.A. Waugh and J.W. Goodby, *Phys. Rev. Lett.* **64**, 1545 (1990); see also P.G. de Gennes, *Solid State Commun.* **10**, 753 (1972).
- [3] P.G. de Gennes and J. Prost, *The Physics of Liquid Crystals*, Second ed., (Oxford University Press, New York, 1993).
- [4] For a more detailed discussion, see R.D. Kamien and D.R. Nelson, Institute for Advanced Study Preprint IASSNS-HEP-94/68 and in preparation.
- [5] V.L. Indenbom and A.N. Orlov, *Usp. Fiz. Nauk* **76** 557 (1962) [*Sov. Phys. Uspekhi* **5** 272 (1962)].
- [6] M.C. Marchetti and D.R. Nelson, *Phys. Rev. B* **41** 1910 (1990).
- [7] M. Kléman and P. Oswald, *J. Phys. (Paris)* **43** 655 (1982).
- [8] W.A. Bollman, *Crystal Defects and Crystalline Interfaces*, (Springer-Verlag, Berlin, 1970); J.P. Hirth and J. Lothe, *Theory of Dislocations*, Second ed. (Wiley, New York, 1982).
- [9] D.C. Wright and N.D. Mermin, *Rev. Mod. Phys.* **61**, 385 (1989); see also M. Kléman, *J. Phys. (Paris)* **46**, 1193 (1985).

## Figure Captions

- Fig. 1. A single screw dislocation in a polymer crystal. The dark horizontal line is the screw dislocation.
- Fig. 2. The smectic twist grain boundary state. Each plane is a smectic layer and each stack is separated by a smectic Twist Grain Boundary. Figure provided courtesy of Tom Lubensky.
- Fig. 3. A single moiré map for triangular lattices with  $n = 1, 2, 3, 4$  ( $\phi_n = 21.8^\circ, 13.2^\circ, 9.4^\circ, 7.3^\circ$  respectively). The crosses can be thought of as the ends of polymers in a perfect crystalline region, as can the circles. They join by connecting to the nearest polymer in order to reduce the elastic energy. The shaded lines are the screw dislocations which make up a honeycomb network.
- Fig. 4. The projected top view of a moiré map on a square lattice with rotation angle  $\tan^{-1}(3/4)$ . The four boxes show the projected polymer paths after  $p = 1, 2, 3, 4$  iterations.
- Fig. 5. The moiré state. The thick tubes running in the  $\hat{z}$  direction are polymers, while the dark lines are stacked honeycomb arrays of screw dislocations. The intersection of these polymers with any constant  $z$  cross section away from the hexagonal defect arrays forms a perfect triangular lattice.
- Fig. 6. Phase diagram of a chiral polymer crystal. Insets are representative tilt (TGB) and moiré grain boundaries. Shaded lines are screw dislocations.
- Fig. 7. A projected top view of 40 random polymers paths resulting from the moiré map with  $n = 1$  iterated 99 times. There is an exceptional fixed point of all 99 maps at the center.

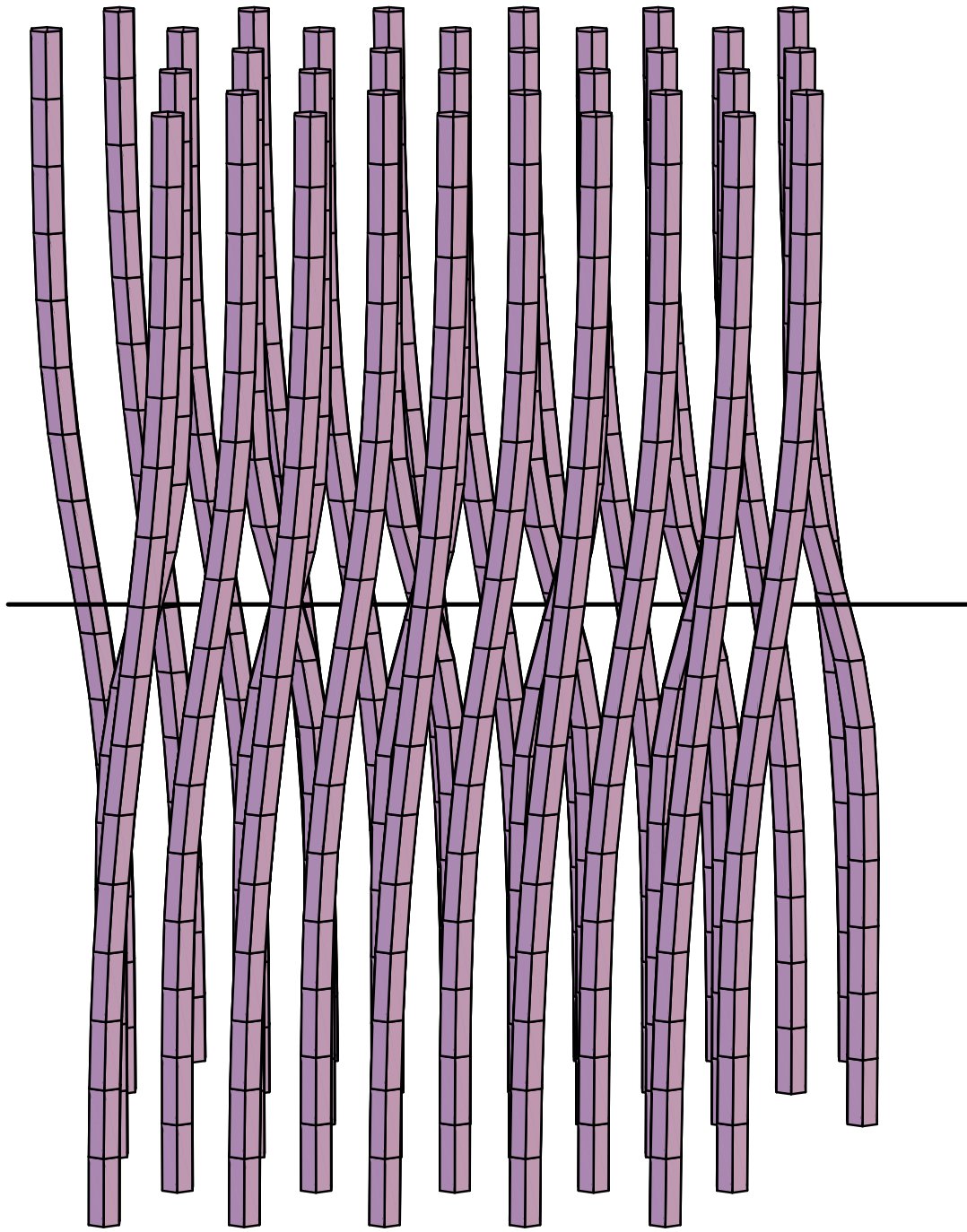


**Figure 1**

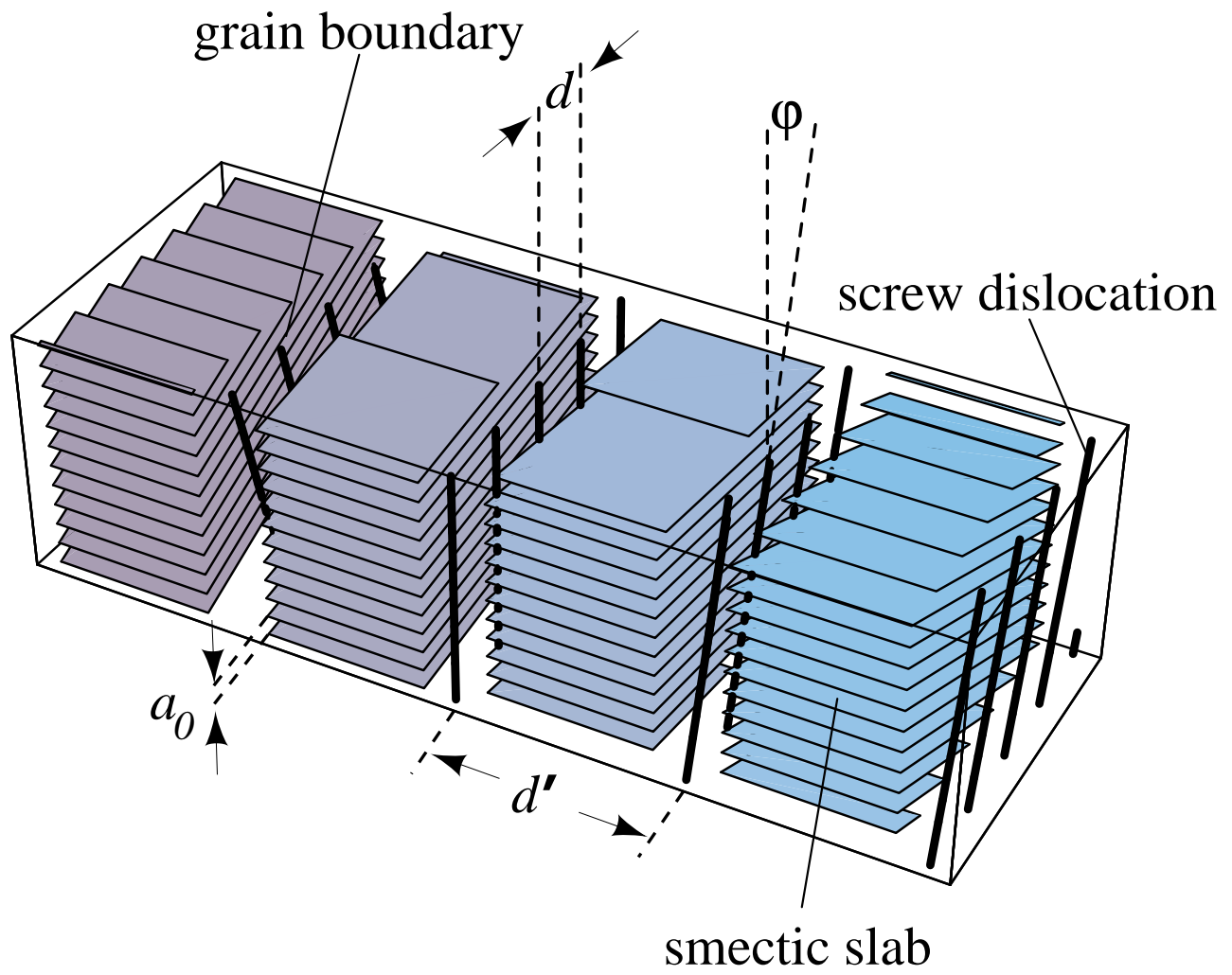


**Figure 2**

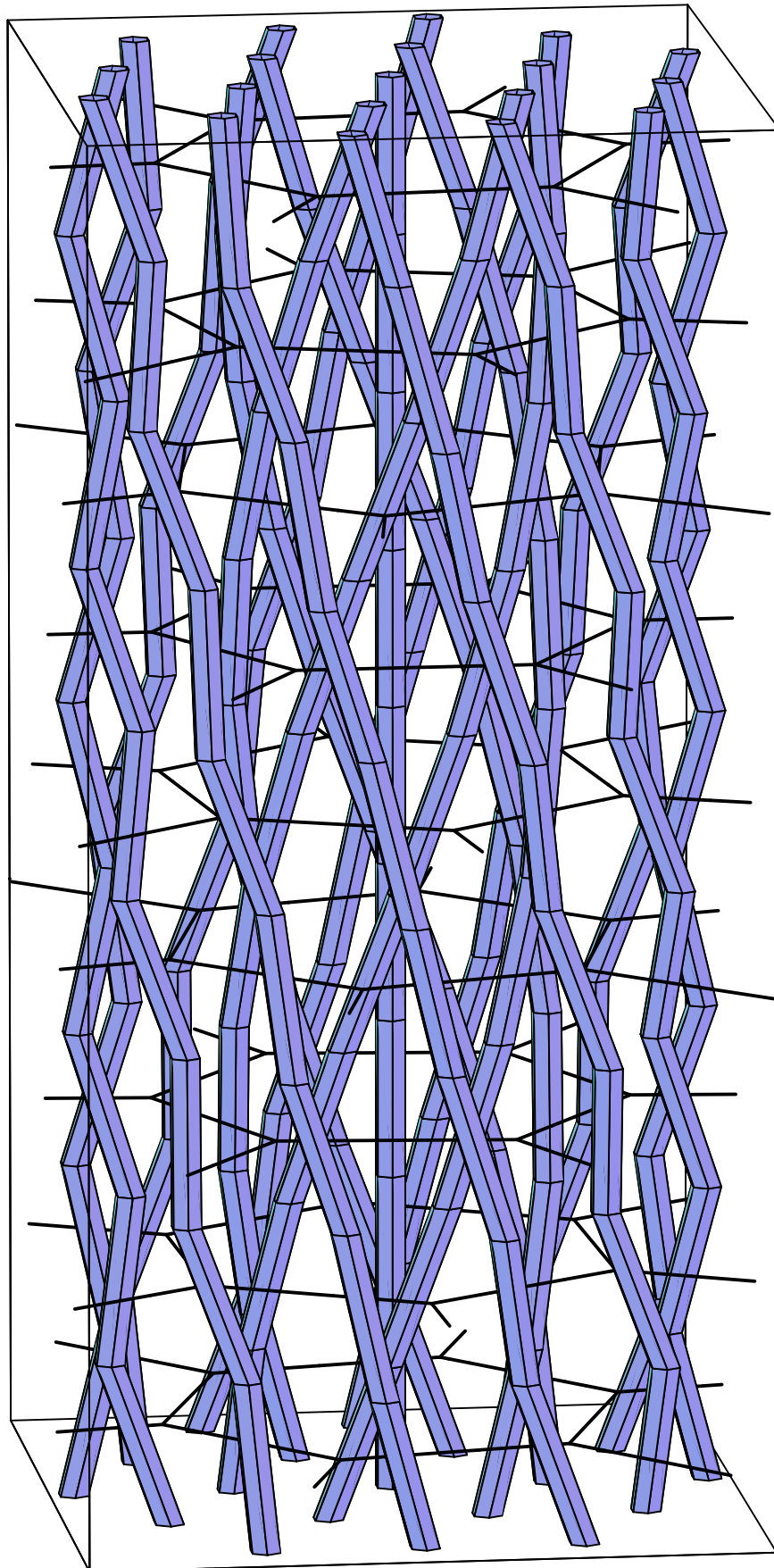


**Figure 5**

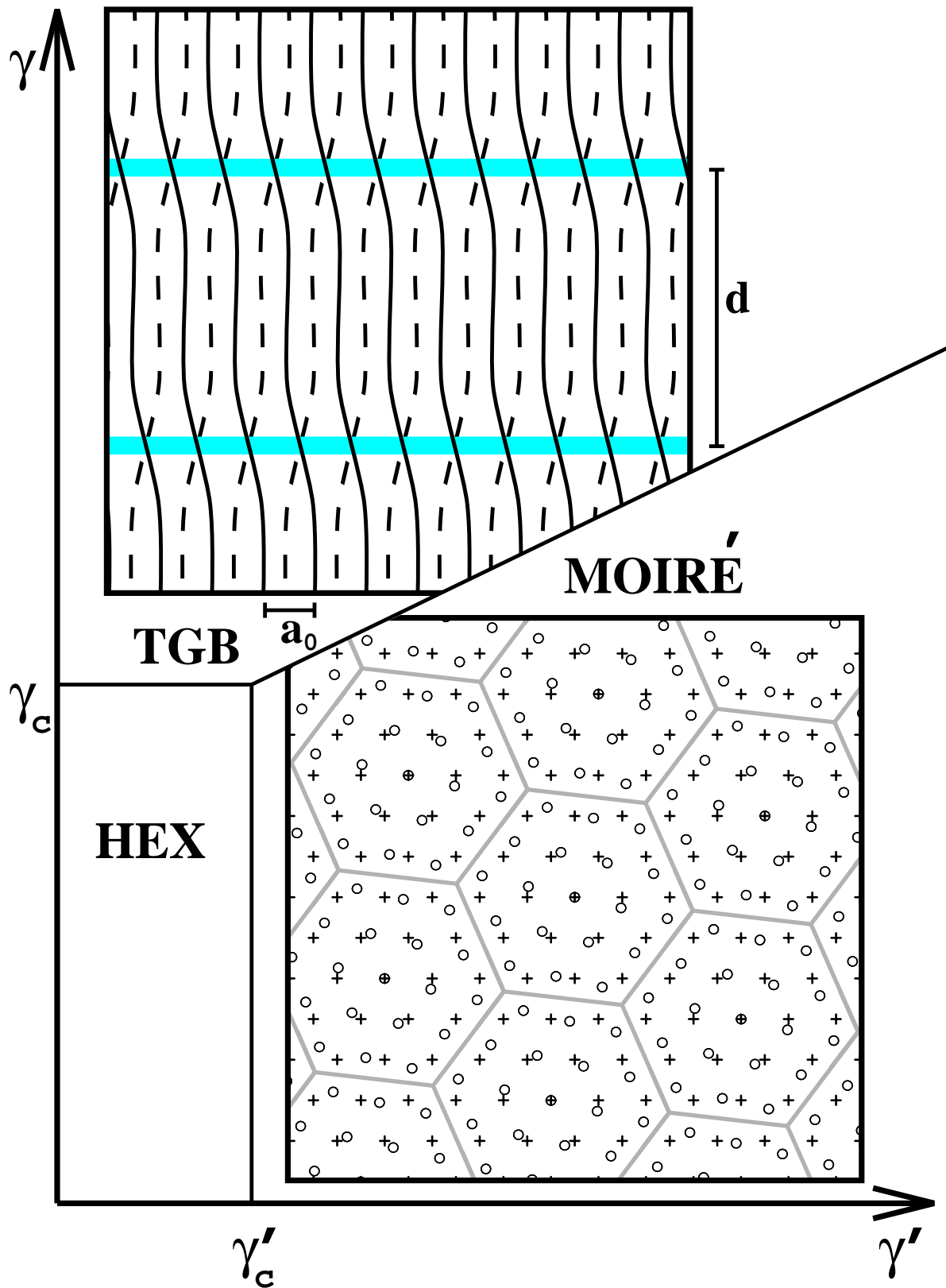


**Figure 6**



**Figure 7**